Clinical and Experimental Immunology, 2022, **207**, 307–317
https://doi.org/10.1093/cei/uxac006
Advance access publication 17 January 2022
Research Article

Clinical & Experimental IMMUNOLOGY

OXFORD

Research Article

Extracellular vesicles containing PD-L1 contribute to CD8+ T-cell immune suppression and predict poor outcomes in small cell lung cancer

Xiaoyan Dou[1,#], Yan Hua[1,#], Zhaowu Chen[1], Fengmei Chao[2], and Ming Li[1,*]

[1]Department of Laboratory Diagnostics, The First Affiliated Hospital of USTC, Division of Life Sciences and Medicine, University of Science and Technology of China, Hefei, China
[2]Department of Cancer Epigenetics Program, The First Affiliated Hospital of USTC, Division of Life Sciences and Medicine, University of Science and Technology of China, Hefei, Anhui, China

[*]Correspondence: Department of Laboratory Diagnostics, The First Affiliated Hospital of USTC, Division of Life Sciences and Medicine, University of Science and Technology of China, Hefei, China, 230032. Email: liming19831002@163.com
[#]Co-first author

Abstract

Programmed death ligand-1 (PD-L1) is expressed on the surface of tumor cells and binds to programmed cell death protein-1 (PD1) on the surface of T cells, leading to cancer immune evasion via inhibition of T-cell function. One of the characteristics of small cell lung cancer (SCLC) is its ineffective anti-tumor immune response and highly immunosuppressive status in the tumor microenvironment. SCLC cells have been shown to generate extracellular vesicles (EVs), which may play an important role in tumor progression. We thus hypothesized that SCLC EVs may be important mediators of immunosuppression and that PD-L1 could play a role. Herein, we showed that PD-L1 was expressed on the surface of SCLC-derived EVs, with the potential to directly bind to PD1. Experimentally, we further showed that EVs secreted by SCLC cells can inhibit CD8+ T-cell activation and cytokine production *in vitro* in response to T-cell receptor stimulation. Importantly, an anti-PD-L1 blocking antibody significantly reversed the EV-mediated inhibition of CD8+ T-cell activation. Furthermore, we performed a retrospective study of patients with SCLC to determine the prognostic value of PD-L1 harvested from plasm circulating EVs. The results showed that EVs containing PD-L1 was an independent prognostic factor and significantly correlated with progression-free survival. Together, these results indicate that EVs containing PD-L1 can be served as a diagnostic biomarker for predicting the effectiveness of therapy, as well as a new strategy to enhance T-cell-mediated immunotherapy against SCLC cancers.

Keywords: extracellular vesicles, programmed death-ligand 1, CD8+ T cell, immune suppression, clinical significance, small cell lung cancer

Abbreviations: SCLC: small cell lung cancer; HD: healthy donors; PFS: progression-free survival; ICI: immune checkpoint inhibitor; PD-L1: PD-1 ligand; EVs: extracellular vesicles; PBS: phosphate-buffered saline; TEM: transmission election microscopy; ROC: receiver operating characteristic; NC: negative control; nFCM: nano-flow cytometer; IL-2: interleukin-2

Introduction

Small cell lung cancer (SCLC) is a major public health problem worldwide, accounting for ~15% of all lung malignancies. SCLC is highly lethal, and most patients die within 1 year of diagnosis [1, 2]. Despite continuing efforts to develop new therapies, the 5-year overall survival rate for patients with extensive-stage SCLC has remained at ~5% for several decades. Treatment failures have largely been attributed to the early development of widespread metastases leading to an extremely poor prognosis [3, 4]. Patients with advanced SCLC are thought to mount a weak and ineffective anti-tumor immune response, which contributes to the highly immunosuppressive status of the tumor microenvironment and promotes tumor progression [5, 6].

Immune checkpoint inhibitor (ICI) targeting PD-1 ligand (PD-L1) has become first- or second-line treatments for the management of several types of cancer, particularly melanoma and lung cancer [7–9]. In the IMpower 133 double-blind study of patients with extensive-stage SCLC, the median overall survival and PFS were significantly longer for the atezolizumab group than the placebo group [10, 11]. Despite these promising results, the general prognosis for SCLC patients remains dismal [12]. A recent single-group phase 2 trial of maintenance pembrolizumab in patients with extensive-stage SCLC failed to demonstrate longer PFS or overall survival compared with historical data [13]. One possible explanation for the variable effectiveness of ICI in SCLC patients is the lack of biomarkers to predict response to these drugs. Thus, there is an urgent need to validate novel biomarkers to identify patients who will most benefit from this immunotherapeutic approach.

Previous studies have shown that patients with lung cancer who have elevated levels of PD-L1 at the tumor-stromal

Received 11 August 2021; Revised 21 December 2021; Accepted for publication 12 January 2022

interface have especially poor outcomes [13]. However, the reported levels of PD-L1 expression are highly variable, due to differences in techniques used to quantify PD-L1 and their associated limitations associations [13, 14]. A recent study using mouse models showed that prostate cancer cells secrete PD-L1 in extracellular vesicles (EVs). Furthermore, removal of EV PD-L1-inhibited tumor growth, even in models resistant to anti-PD-L1 antibodies [15]. This study suggested that quantification of EV PD-L1 may be a useful method for evaluating the efficacy of cancer treatments.

EVs are small vesicles (30–150 nm) with a lipid bilayer membrane that are produced and released by all cells through a defined intracellular trafficking route [16]. Because EVs are stable and not easily degraded by proteolytic enzymes, tumor-secreted EVs are currently emerging as critical messengers in tumor progression and metastasis and in modulation of the host immune system [17–22]. In recent studies of cancer patients, EV PD-L1 were shown to be an effective predictor of anti-PD-1 therapy [23–25]. Other studies have shown that EV PD-L1 can inhibit T-cell-mediated killing of breast cancer cells and promote tumor growth in breast cancer models [19]. Monitoring of circulating EV PD-L1 may also be useful to predict the tumor response to treatment and clinical outcome in melanoma patients [26]. However, whether circulating EV PD-L1 could be used as a prognostic factor in SCLC patients is unknown. Moreover, it is also unclear whether EV PD-L1 retains its ability to act as an immunosuppressant in SCLC.

In this study, we reported that the expression of PD-L1 was a significant difference between SCLC tumor cells. EV from SCLC cells suppressed the activation and function of $CD8^+$ T cells in a PD-L1-dependent manner. It suggested that SCLC tumor cell-derived EVs could create an immunosuppressive microenvironment for SCLC progression. Subsequently, we investigated the association between disease progression and circulating EV PD-L1 levels in SCLC patients. Of clinical interest, our results indicated that EV PD-L1, but not total plasma PD-L1, correlate significantly with disease activity. EV PD-L1 was an independent prognostic and significantly correlated with PFS. Together, these findings revealed that EV PD-L1 exerts a crucial role in SCLC progression, and could serve as a diagnostic biomarker for SCLC.

Materials and methods

Study participants

This retrospective study was conducted between December 2016 and December 2018 in the Department of Respiratory Oncology, Western Branch of The First Affiliated Hospital of the University of Science and Technology of China, China. Clinicopathological data from patients with SCLC (n = 70), including age, gender, smoking history, disease status, and distant metastasis, were collected from medical records. PFS was defined as the time from treatment initiation to recurrence or the date of censorship (date of the last follow-up).

Cell culture

Human SCLC cell lines H82, H69, DMS273, SHP77, H446, and SBC-3 were purchased from the American Type Culture Collection (Manassas, VA, USA). The cells were cultured in RPMI-1640 medium (Hyclone) supplemented with 10% EV-depleted fetal bovine serum (Gibco) and were maintained at 37°C in a 5% CO_2 atmosphere. All cell lines were tested for mycoplasma contamination.

Isolation of EVs from patient plasma and cell culture medium

Peripheral blood was drawn into EDTA-K_2 tubes and centrifuged at 3155g for 10 min. The supernatants were then removed and centrifuged at 3000g for 10 min, and the clarified plasma was removed and stored at −80°C until further processing. Thawed plasma samples were differentially centrifuged at 16 400g for 45 min at 4°C. The supernatants were removed and ultracentrifuged at 130 000g for 1 h at 4°C (Beckman Coulter Optima L-100XP). The supernatants were discarded and the EV pellets were washed with 1 ml phosphate-buffered saline (PBS). Then, the media was filtered using a 0.22-μm pore filter, followed by a second step of ultracentrifugation at 130 000g for 1 h at 4 °C. Afterward, the supernatant was discarded, and the EVs were suspended either in 100 μl of 1× PBS.

SBC-3 cells were resuspended in RPMI-1640 medium containing exosome-depleted FBS and cultured until they reached 80%–90% confluency. The culture supernatants were collected and sequentially centrifuged at 1000g for 10 min and 3000g for 10 min. The supernatant was filtered using a 0.22-μm filter and then ultracentrifuged at 130 000g for 1 h at 4°C (Beckman Coulter, Optima MAX-XP). The supernatant was discarded, and the EV pellet was suspended in either 40 μl of 1% RIPA lysis buffer or 40 μl of PBS.

Characterization of EVs

For transmission electron microscopy (TEM), 2.5 μl aliquots of SBC-3 cell-derived EVs in PBS were pipetted onto 200 mesh formvar/carbon grids that had been hydrophilized for 10 s. Samples were incubated for 90 s and then negatively stained with a 2% phosphotungstic acid solution. Data were acquired using a TEM operating at 120 keV equipped with an UltraScan 1000 CCD Camera (FEI). EV size was measured using a scale bar. Size distribution of SBC-3 cell-derived EVs was performed by nano-flow cytometer (nFCM) analysis [27].

To determine PD-L1 expression on the surface of the EV, single EVs were analyzed by confocal fluorescence microscopy. SBC-3 cells-derived EVs were incubated with anti-human PD-L1 antibody (ab213524) or anti-human anti-CD63 (H5C6) antibody (Novus; NBP2-42225) at 1:200 dilution at room temperature for 2 h and then ultracentrifuged at 130 000g for 1 h at 4°C. The supernatants were removed and the EV pellets were incubated with Alexa Fluor 647-conjugated or Alexa Fluor 488-conjugated secondary antibodies at room temperature for 1 h in the dark. The samples were then ultracentrifuged as indicated above. The supernatants were removed, and the EV pellets were washed with PBS and ultracentrifuged as indicated above. The pellet was resuspended in PBS and applied to a microscope slide precoated with poly-lysine to enable capture of individual EVs. Expression of PD-L1 and CD63 were analyzed using a Nikon Eclipse TI microscope (Nikon 100 × 1.49 NA objective lens model) equipped with a NEO-5.5-CL3 camera. Fluorescence intensity was measured using ImageJ software. Half-height width analysis was performed using MATLAB with a specific analysis code.

Peripheral blood mononuclear cell isolation and functional assays

Peripheral blood mononuclear cells (PBMCs) were isolated from blood samples obtained from healthy donors by centrifugation on Ficoll-Hypaque gradients then and cultured in RPMI-1640 medium supplemented with 10 mM HEPES buffer, 5×10^{-5} M β-mercaptoethanol, 10% FBS, and 1% penicillin/streptomycin. Aliquots of 5×10^5 PBMCs per well were plated in 96-well U bottom plates and incubated with anti-CD3 monoclonal antibody (10 μg/ml; BioLegend, #317326), anti-CD28 antibody (2 μg/ml; BioLegend, #302933) and EVs derived from SBC-NC, SBC-3-PD-L1, DMS273-NC, or DMS273-PD-L1 cell lines. EVs were pretreated with isotype control or 20 mg/ml of anti-PD-L1 antibody (B7-H1) (BioXcell, BE0285) overnight at 4°C. The cells were incubated for 48 h. The PBMCs were harvested and incubated with FITC-conjugated anti-CD8 antibody (BioLegend, #300906) and APC-conjugated anti-CD69 antibody (BioLegend, #310904). The cells were analyzed on an LSRFortessa flow cytometer (BD Biosciences) with gates set on CD8+ T cells. Data were analyzed with FlowJo software.

PBMC culture supernatants collected at the end of the 48 h incubation were analyzed for cytokines using human cytokine Multi-microsphere flow immunofluorescence (RAISECARE) according to the manufacturer's instructions.

Cytotoxic potential assay

PBMCs were isolated from blood samples obtained from healthy donors by centrifugation on Ficoll-Hypaque gradients. Aliquots of 5×10^5 PBMCs per well were placed in 96-well U bottom plates and incubated with anti-CD3 monoclonal antibody (10 μg/ml; BioLegend, #317326), anti-CD28 antibody (2 μg/ml; BioLegend, #302933) and EVs derived from SBC-NC or SBC-3-PD-L1 cell lines. The PBMCs were harvested after incubated for 24 h. The levels of intracellular granzyme B and perforin in CD8+ T cells were evaluated by staining cells with antibodies against human granzyme B or perforin according to the manufacturer's instructions (RAISECARE, #210905) and analyzed by flow cytometry (RAISECARE).

Quantitative reverse-transcription PCR (qRT-PCR)

Total RNA was isolated from cultured cells using TRIzol reagent (Invitrogen, #15596-026) and reverse-transcribed using HiScript II Q-RT SuperMix (Vazyme, #R222-01). Real-time PCR was conducted using a Roche LightCycler 480 system. Gene-specific primers were designed using Primer 5 software as follows: PD-L1: 5′-GGCATTTGCTGAACGCAT-3′ (forward) and 5′-CAATTAGTGCAGCCAGGT-3′ (reverse); glyceraldehyde 3-phosphate dehydrogenase (GAPDH): 5′-AACGGATTTGGTCGTATTG-3′ (forward) and 5′-GGAAGATGGTGATGGGGAT-3′ (reverse).

Cell viability assay

Cell viability was measured using a Cell Counting Kit 8 (CCK8; Beyotime Biotechnology). In brief, cells were plated at 4×10^3/100 μl/well in 96-well plates and incubated for 24, 48, or 72 h. CCK-8 reagent was added at 10 μl/well and the plate was incubated for 2 h at 37°C. Absorbance at 450 nm was read using a Tecan Reader system.

PD-L1 enzyme-linked immunosorbent assay

Total plasma PD-L1 and EV PD-L1 were measured using a Quantikine ELISA kit (R&D Systems, #DB7H10) according to the manufacturer's instructions. In brief, 100 μl of sample per well was added to the enzyme-linked immunosorbent assay (ELISA) plate and incubated for 2 h at room temperature. The wells were washed with 400 μl Wash Buffer, 200 μl/well human PD-L1 detection antibody was added, and the plates were incubated for an additional 2 h at room temperature. Substrate solution (200 μl/well) was then added and the plates were further incubated for 30 min at room temperature. The reaction was stopped by the addition of a 50 μl Stop Solution. The absorbance at 450 nm was measured using a microplate reader. PD-L1 concentrations were calculated from standard curves.

Western blot analysis

SCLC cells or EVs were incubated in RIPA lysis buffer for 15 min and centrifuged. Lysate samples were separated by SDS–PAGE, and proteins were transferred to polyvinylidene fluoride membranes (Millipore). The membranes were blocked with 5% bovine serum albumin for 1 h and then incubated overnight at 4°C with primary antibodies specific for TSG101 (Novus, #NBP1-80659), PD-L1 (Abcam, #ab213524), CD63 (H5C6) (Novus, #NBP2-42225), calnexin (CST, #2679T), or GAPDH (Sigma–Aldrich, #A3854). The membranes were washed and incubated with horseradish peroxidase-conjugated secondary antibody (Beyotime Biotechnology) for 1 h at room temperature. Immunoreactive proteins were revealed using ECL detection reagents (Beyotime Biotechnology). Band intensities were quantified using a Tanon Imaging System.

Statistical analysis

Statistical analysis was performed using Prism 5 software (GraphPad). Relationships between variables were examined using Spearman's correlation coefficient. Results from Cox proportional hazards models are reported as hazard ratios (HRs) with 95% confidence intervals (CIs). Survival analysis was performed using the Kaplan–Meier method, and differences were assessed using a two-tailed log-rank test. Receiver operating characteristic (ROC) curve area analysis was used to measure the predictive power of EV PD-L1 by determining the area under the curve (AUC). Data are presented as the mean ± standard deviation (SD) from at least three independent experiments. For normally distributed data, mean differences were analyzed using two-tailed paired or unpaired Student *t*-tests. A two-tailed value of $P < 0.05$ was considered statistically significant.

Results

Cultured SCLC cell lines release EVs expressing membrane PD-L1

To analyze SCLC tumor cell-derived EVs in more detail, we first selected a cell line that expressed high levels of PD-L1 from among a panel of six SCLC cell lines (H82, H69, DMS273, SHP77, H446, and SBC-3) using Western blot analysis. As shown in Fig. 1A, PD-L1 expression was detected only in DMS273 and SBC-3 cells; of these, SBC-3 cells showed the highest expression. SBC-3 cells were cultured to 80%–90% confluency and EVs were purified from

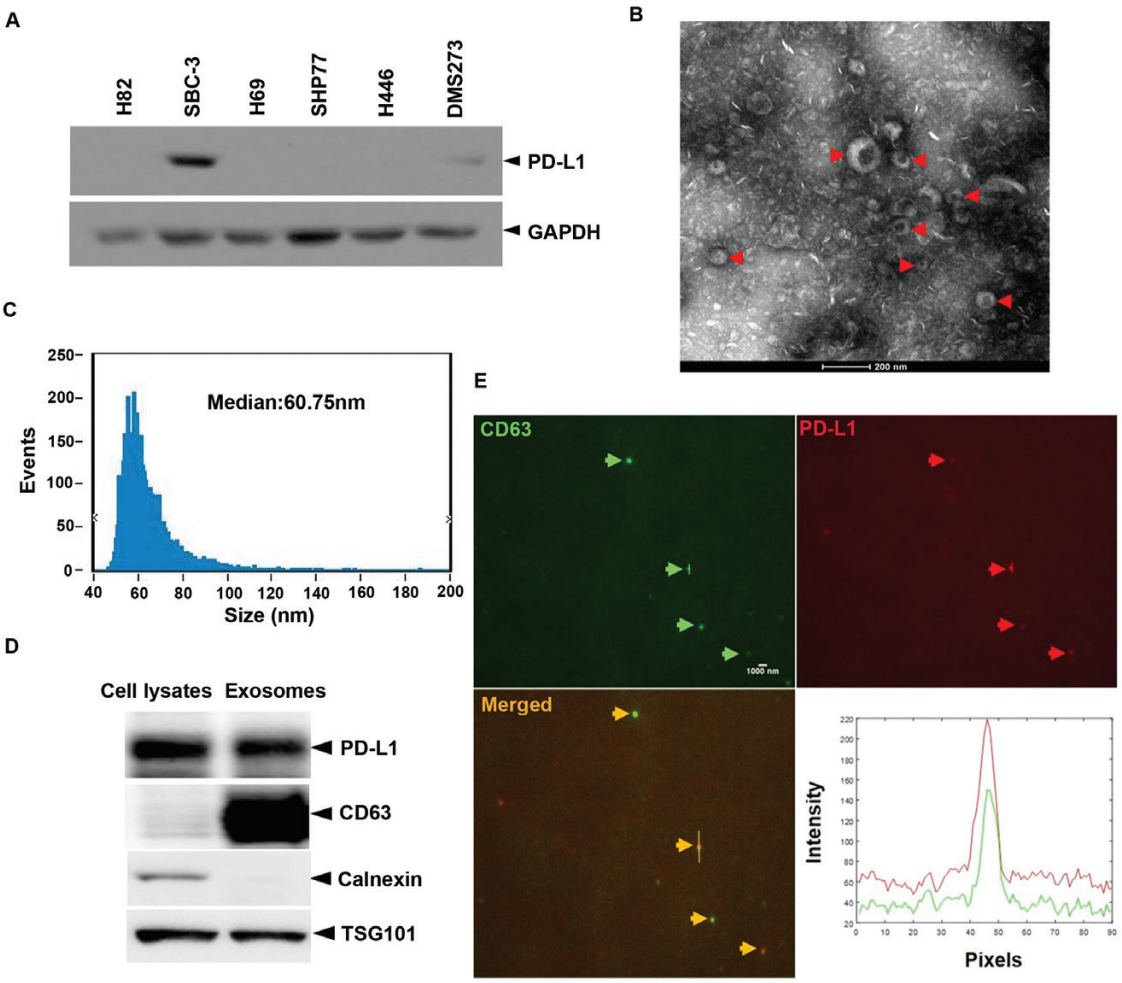

Figure 1: SCLC tumor cells release EVs expressing membrane PD-L1. (A) Western blot analysis of the expression of PD-L1 in multiple lung cancer cells. (B) A representative TEM image of purified SBC-3 cells EVs. Red arrows point to EVs. (C) Size distribution of SBC-3-derived EVs, as analyzed by nFCM. (D) Western blot of PD-L1 in EVs isolated from the media of SBC-3 and SBC-3 cells. CD63 and TSG101, the markers of EVs. Calnexin, the negative marker of EVs. (E) Representative confocal immunofluorescence microscope image showing expression levels of CD63 (EVs marker, displaying with green fluorescence) and PD-L1 (displaying with red fluorescence) on the surface of single EV isolated from SBC-3 cells. Arrows point to EVs.

the resulting culture supernatant. TEM of the SBC-3-derived EVs revealed a saucer-like morphology (Fig. 1B), and nano-flow cytometer (nFCM) analysis showed that the vesicles were approximately 60.75 nm in diameter (Fig. 1C). Analysis of EVs by Western blotting demonstrated that PD-L1 was co-expressed with TSG101 and CD63, two markers of EVs (Fig. 1D). Furthermore, the expression of endoplasmic reticulum-specific protein calnexin was negative in EVs (Fig. 1D). Finally, we examined the localization of PD-L1 by labeling the EVs with anti-PD-L1 and anti-CD63 antibodies followed by confocal fluorescence microscopy. As shown in Fig. 1E, PD-L1 co-localized with the membrane marker CD63 in EVs, indicating the presence of PD-L1 in the EVs' membrane.

SCLC cell-derived PD-L1$^+$ EVs suppress CD8$^+$ T-cell function *in vitro*

We next determined whether PD-L1 on the surface of EVs retained the ability to engage cell surface PD-1 and suppress the functions of CD8$^+$ effector T cells. We first established SBC-3 and DMS273 cells lines expressing empty vector (SBC-3-NC and DMS273-NC) or a PD-L1 expression vector (SBC-3-PD-L1 and DMS273-PD-L1). As shown by Western blot and qRT-PCR analysis, PD-L1 protein and mRNA expression, respectively, were strongly upregulated in SBC-3-PD-L1 and DMS273-PD-L1 cells compared with negative control (Fig. 2A). We then determined the effect of PD-L1 overexpression on cell proliferation in SCLC cells. As shown in Fig. 2B, overexpression of PD-L1 had no significant effect on the cell proliferation neither in SBC-3 nor DMS273 cell lines. Compared with the size distribution of SBC-NC EVs, with a median size of 60.75 nm, the particle size distribution of EVs isolated from SBC-3-PD-L1, with a median size was measured to be 62.75 nm (Figs. 1C and 2C). Accordingly, EVs secreted by PD-L1-overexpressed cells also contained higher levels of PD-L1 compared with EVs derived from NC cells in SBC-3 and DMS273 (Fig. 2D). Importantly, PD-L1 was expressed higher in EVs derived from SBC-3-PD-L1 cells than EVs from SBC-3-NC cells analyzed by nFCM (12.7% vs 9.92%) (Fig. 2E).

EV PD-L1 derived from multiple types of cancer cells have been shown to affect T-cell functions [19, 24, 28, 29]. Therefore, we next investigated the effects of SBC-3-derived EVs on CD8$^+$ T-cell activation and cytokine secretion. PBMCs were isolated from healthy donors and incubated for 48 h with anti-CD3/anti-CD28 antibodies with or without EVs purified

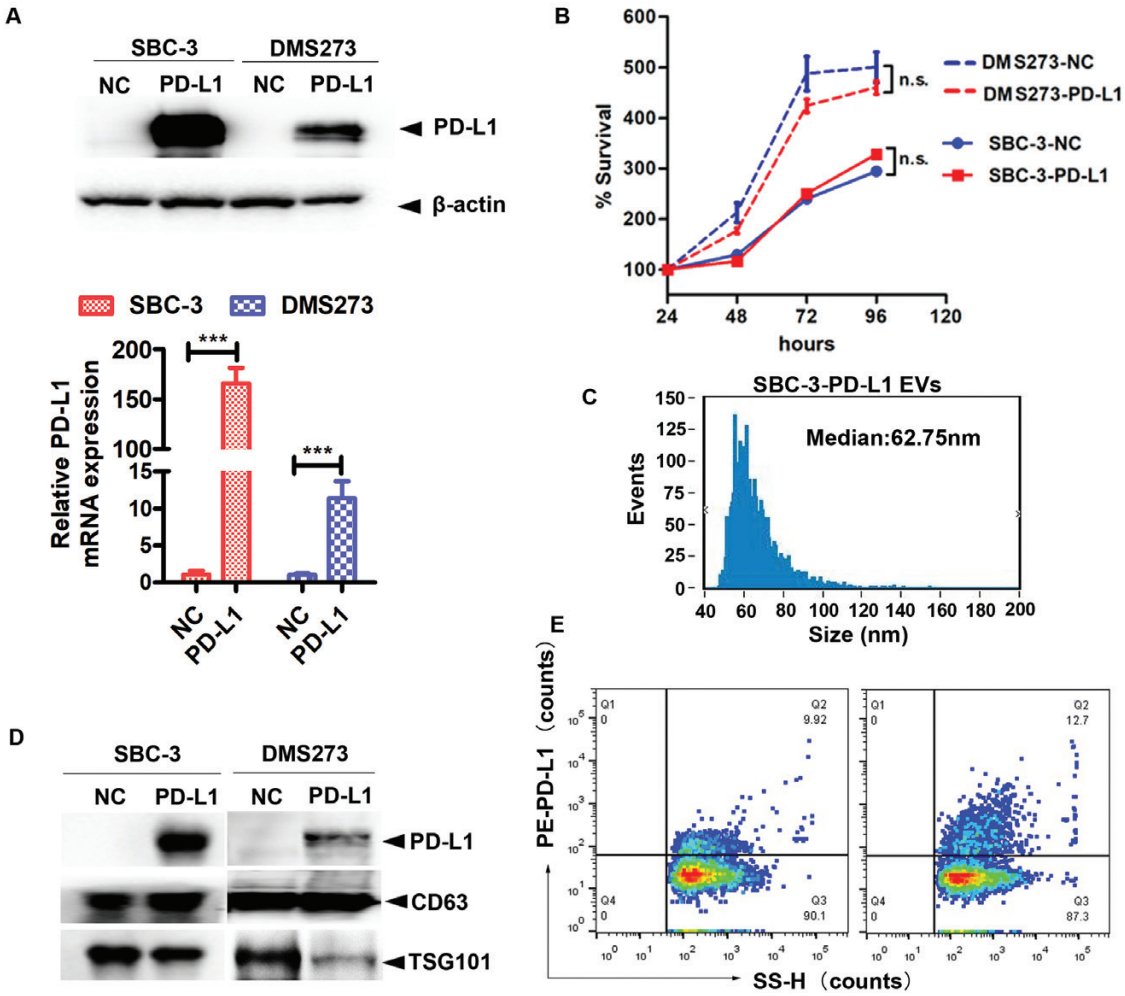

Figure 2: EVs containing PD-L1+ downregulate CD69 expression on effector CD8+ T cells. (A) The PD-L1 in SBC-3 and DMS273 cells was analyzed by Western blot analysis after transfection with NC or PD-L1 (upper). Relative mRNA amounts of PD-L1 in SBC-3-NC, SBC-3-PD-L1, DMS273-NC, and DMS273-PD-L1 cells. The amounts of mRNA from the gene of interest were normalized to GAPDH (lower). (B) The effect of PD-L1 overexpression on SBC-3 and DMS273 cell proliferation was determined by the cell viability assay. (C) Size distribution of SBC-3-PD-L1-derived EVs, as analyzed by nFCM. (D) Immunoblots for PD-L1 in purified EVs from SBC-3-NC, SBC-3-PD-L1, DMS273-NC, and DMS273-PD-L1 cells. The same amounts of proteins were loaded for each fraction. (E) The PD-L1 in EVs harvested from SBC-3-NC and SBC-3-PD-L1 cells were analyzed by nFCM. The preparation of EVs from culture medium was fluorescently labeled with PE-conjugated mAbs specific to PD-L1. The percentage of phenotype-positive EVs was provided in the plot.

from NC or PD-L1 overexpressed cells. CD8+ T-cell activation status (CD69 expression) and effector function (cytokine secretion) were then analyzed by flow cytometry. Cells stimulated in the presence of SBC-3-NC- or DMS273-NC-derived EVs exhibited increased CD69 expression and cytokine secretion, as expected (Fig. 3A–C). However, the presence of SBC-3-PD-L1- or DMS273-PD-L1-derived EVs significantly reduced the expression of CD69 and secretion of interleukin-2 (IL-2) (Fig. 3C). Interestingly, SBC-3-PD-L1-derived EVs increased CD8+ T-cell secretion of IL-10 and IL-17 (Fig. 3C), which have been shown to be key promoters of cancer growth *via* their effects on the activities of myeloid and T cells [30–32].

Currently, granzyme B and perforin are considered to be key anti-tumor effector molecules in T lymphocytes [33, 34]. Perforin pores facilitate granzyme B entering into the target cell, after which they can induce target cell death [35]. To determine whether PD-L1+ EVs contribute to lower CD8+ T-cell cytotoxic potential, we treated PBMCs with EVs derived from SBC-3-NC and SBC-3-PD-L1 cells for 24 h and measured the intracellular expression of granzyme B and perforin in CD8+ T cells by flow cytometry. We found that the percentages of granzyme B+ CD8+ T cells and perforin+ CD8+ T cells were all significantly decreased following the EV PD-L1+ treatment compared with the NC group (Fig. 3D). Collectively, these results suggest not only that EV PD-L1 is functional but also that it is able to promote T-cell immunosuppression.

EV PD-L1 is associated with clinicopathological characteristics in SCLC

To evaluate EV PD-L1 as a potential biomarker in SCLC, we analyzed blood samples from 30 healthy donors and 70 SCLC patients. The clinical characteristics of the SCLC patients are summarized in Table 1. The study group consisted of 55 men and 15 women with a median age of 65 years (range 47–79 years). At diagnosis, 58.5% of the patients consumed tobacco. At study enrolment, 46 (65.7%) patients had extensive-stage disease and 24 (34.3%) had local-stage disease. None of the patients had received ICIs.

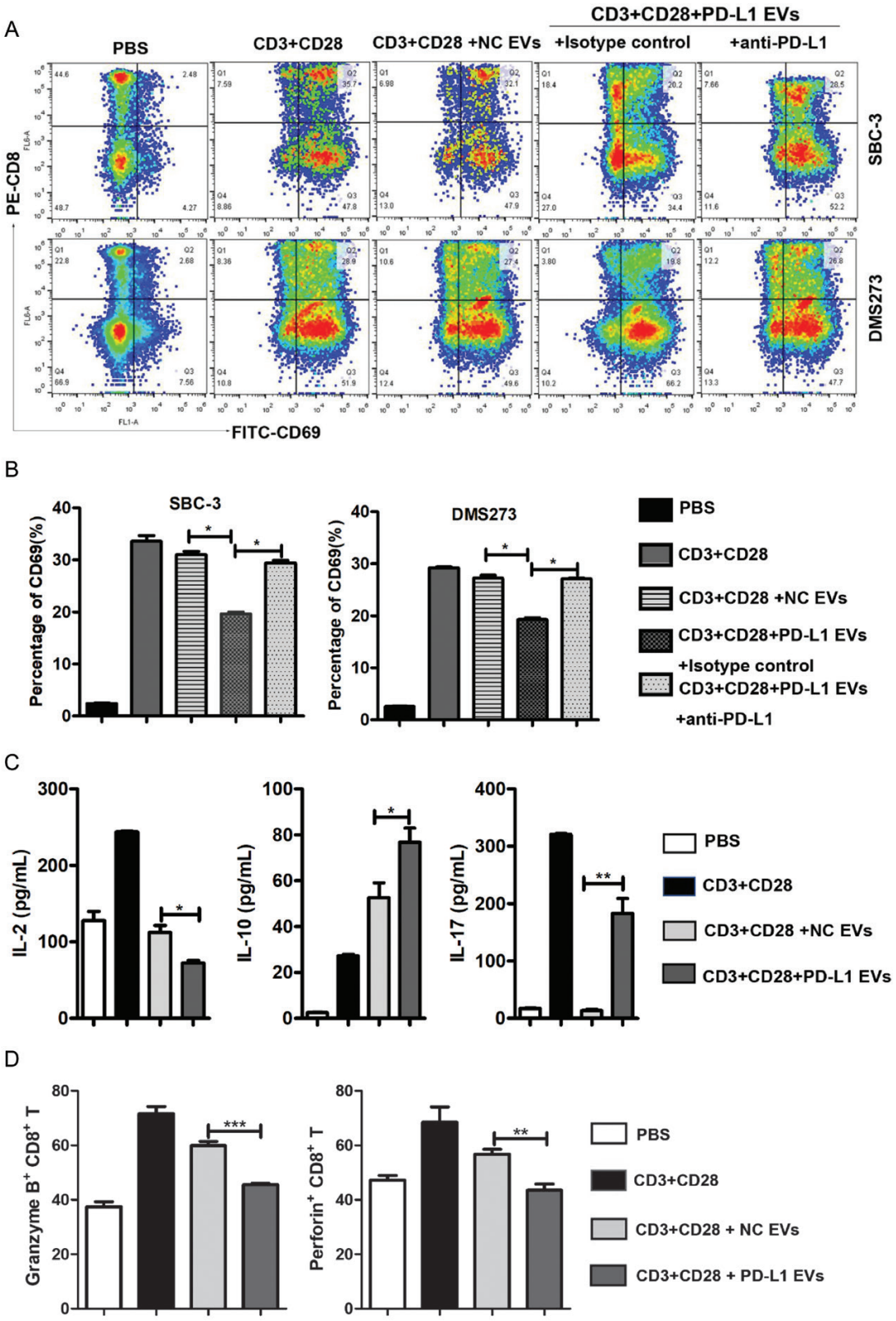

Figure 3: EVs containing PD-L1$^+$ downregulate CD69 expression on effector CD8$^+$ T cells. (A) FACS contour plots showing a frequency of CD8$^+$CD69$^+$ cells in total CD8$^+$ T cells in the PBMCs following various treatments at day 2. Decreasing levels of CD69 expression on CD8$^+$ T cells after co-incubation with PD-L1$^+$ EVs isolated from SBC-3-PD-L1 and DMS273-PD-L1 cells. The results are representative of three independent experiments. (B) Statistical analysis of the difference in expression of CD69 by flow cytometry in CD8$^+$ T cells. $*P < 0.05$. (C) Multi-microsphere flow immunofluorescence assay assessment for secretion of IL-2, IL-17, and IL-10 in human PBMCs (stimulated with anti-CD3/CD28 antibodies) after treatment with SBC-3-NC-derived EVs or SBC-3-PD-L1 cell-derived EVs for 2 days. (D) PBMCs were analyzed by flow cytometry after staining with anti-human antibodies CD8-APC, granzyme B-PE, and perforin-FITC. Histograms represent the mean ± SD of three independent experiments. $**P < 0.01$. $***P < 0.001$.

Table 1: SCLC patients' characteristics according to the expression of PD-L1

Variables	Number of patients(%)	Total PD-L1	EVs PD-L1
		P value	*P* value
Age (years)			
≤ 65	38(54.3)	0.0101	0.0282
> 65	32(45.7)		
Gender			
Male	55(82.9)	0.0863	0.0679
Female	15(17.1)		
Smoking[a]			
Ever	35(58.5)	0.1115	0.9147
Never	35(41.5)		
Disease status			
LD	24(34.3)	0.0035	0.001
ED	46(65.7)		
Distant metastasis			
M0	48(65.9)	0.0925	0.007
MX	22(34.1)		

The *p*-value refers to Student's t-test testing homogeneity of patients' characteristics. Bold values indicate statistical significance(p<0.05).
LD, limited disease; ED, extensive disease; M0, no distant metastasis; MX, distant metastasis.
[a]Smoking status is based on self-reported information.

We next assessed total PD-L1 and EV PD-L1 levels in plasma by ELISA. Total PD-L1 was higher in plasma samples from SCLC patients (n = 70, median 35.477 pg/ml) than in plasma samples from healthy donors (n = 30, median 23.655 pg/ml) (P = 0.0011, Fig. 4A). Interestingly, an even more striking difference between SCLC patients and healthy donors was observed in the level of EV PD-L1 (median 14.07 and 6.515 pg/ml, respectively; P < 0.0001, Fig. 4B). These results indicate that SCLC was associated with a greater change in EV PD-L1 than in total plasma PD-L1.

We next determined whether total or EV PD-L1 levels could discriminate between SCLC patients and healthy donors by performing ROC curve analysis. Total PD-L1 levels showed good discriminatory ability (AUC = 0.7236, SE = 0.071, 95% CI = 0.5842–0.8631; P = 0.003; Fig. 4C), but EV PD-L1 levels showed superior discrimination between the two groups (AUC = 0.8742, SE = 0.045, 95% CI = 0.7859–0.9626; P < 0.0001; Fig. 4D). This analysis indicated that using the optimal cut-off value of 9.326 pg/ml, plasma EV PD-L1 levels could identify SCLC patients with 75.71% sensitivity and 93.33% specificity.

Analysis of clinicopathological characteristics revealed that total plasma PD-L1 levels were not significantly associated with gender, smoking history, or tumor distant metastasis, whereas older age and disease status were associated with a significantly higher total PD-L1 level (P = 0.0101 and P = 0.0035, respectively, Table 1). In contrast, EV PD-L1 level was significantly associated with age (P = 0.0282), disease status (P = 0.001) (Fig. 4F), and distant metastasis (P = 0.007), but not with gender or smoking history (Table 1). These results indicate that plasma EV PD-L1 may be a superior biomarker than total plasma PD-L1for SCLC.

High EV PD-L1 level is associated with shorter PFS

Next, we investigated the PFS of SCLC patients stratified by high/low total plasma PD-L1 level and high/low plasma EV PD-L1 level. Kaplan–Meier survival analysis indicated that PFS was not significantly different for patients in the total PD-L1^{low} and total PD-L1^{high} groups (P = 0.063, Fig. 5A). However, PFS was significantly poorer for patients in the EV PD-L1^{high} group compared with the EV PD-L1^{low} group (HR = 2.857, 95% CI = 1.637–4.984, P = 0.0002) (Fig. 5B). Taken together, these findings suggest that circulating EV PD-L1 levels might be useful to predict clinical outcomes in SCLC.

EV PD-L1 level is a prognostic marker in SCLC

To determine whether EV PD-L1 level could act as a prognostic marker, we evaluated tumor progression or response to therapy using at least two imaging modalities at 1- to 2-month intervals during treatment. In parallel, we quantified EV PD-L1 in plasma samples. As shown in Fig. 6A–C, patients who did not progress during serial monitoring exhibited decreased levels of circulating EV PD-L1 during treatment, and conversely, patients with tumor progression exhibited an increase in circulating EV PD-L1 levels during treatment. Thus, EV PD-L1 could be used as a follow-up marker and predictor of treatment response.

Discussion

EVs are small secreted membrane vesicles that are released extracellularly and enter the systemic circulation [36–39]. Tumor cell-derived EVs could reflect the molecular signature of cancer [17, 40–42]. Most studies suggest that measurement of circulating EV PD-L1 levels may represent a less invasive method than conventional immunohistochemical assays for predicting the prognosis of cancer patients [29, 43–47]. However, the clinical significance of EV PD-L1 and whether EV PD-L1 retained its immunosuppressive properties in SCLC were unclear.

In this study, we showed that total PD-L1 and EVs PD-L1 levels are significantly higher in plasma from SCLC patients than from healthy donors; of these, the difference was greatest for EV PD-L1. PD-L1 expressed by tumor cells has been reported to correlate with poor outcomes after ICI therapy in multiple cancers [24, 26, 28, 48]. In the present study, we did not evaluate PD-L1+ EVs in SCLC patients who were being treated with ICIs; rather, we evaluated changes in EVs PD-L1 levels before and after treatment. We observed that EVs PD-L1 was an independent prognostic factor in SCLC and was significantly associated with disease status. However, the results presented here will need to be confirmed in prospective studies with larger cohorts.

Our results are consistent with a recent report that EVs PD-L1 correlates with disease progression in patients with head and neck squamous cell carcinomas [49]. We observed a significant association between EVs PD-L1 and advanced tumor stage and distant metastasis, whereas total plasma PD-L1 correlated only with advanced age. Moreover, PFS was significantly poorer for patients with high EV PD-L1 levels compared with low levels, indicating that EV PD-L1 might predict survival in the early stages of SCLC. Patients with high plasma EV PD-L1 also had more active and advanced disease than did patients with lower levels.

Previous studies have identified removal of EV PD-L1 from tumor microenvironment was shown to inhibit the growth of prostate tumors, even in the models resistant to anti-PD-L1 antibodies [15]. This study indicated that measurement of EV PD-L1 levels may be useful for evaluating therapeutic efficacy. However, current methods of EVs analysis have not been used

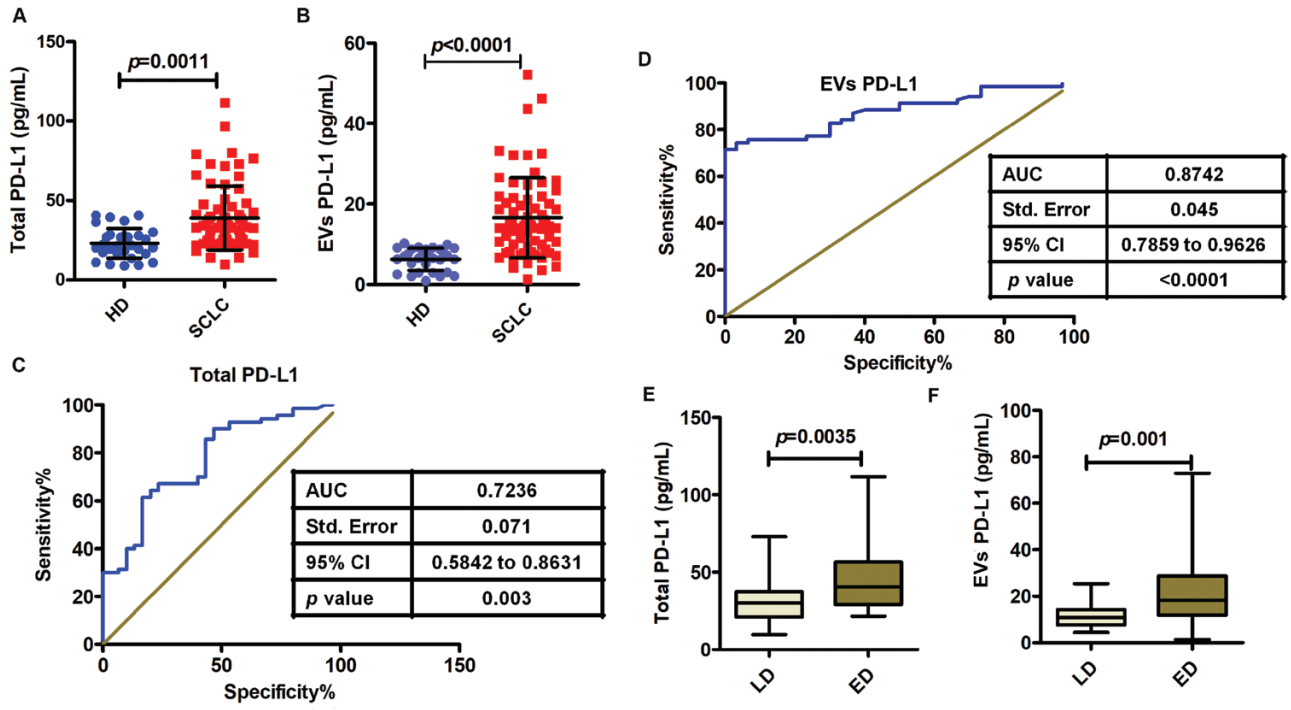

Figure 4: Association of total PD-L1 or EVs PD-L1 levels with clinicopathological data in SCLC. (A) Total PD-L1 is elevated in SCLC patients (n = 70) compared with healthy donor (n = 30) (P = 0.0011). (B) PD-L1$^+$ EV is significantly higher in SCLC patients (n = 70; P < 0.0001). (C and D) ROC curve analysis for the indicated parameters in patients with SCLC compared to healthy donors. (E) Protein concentrations of total PD-L1 show a significant difference in patients with extensive disease (ED) relative to those with limited disease (LD) (P = 0.0035). (F) PD-L1$^+$ EVs are significantly elevated in ED patients compared with LD patients (P = 0.001). Data represent mean ± SD. Statistical analyses were performed using a two-sided unpaired t-test.

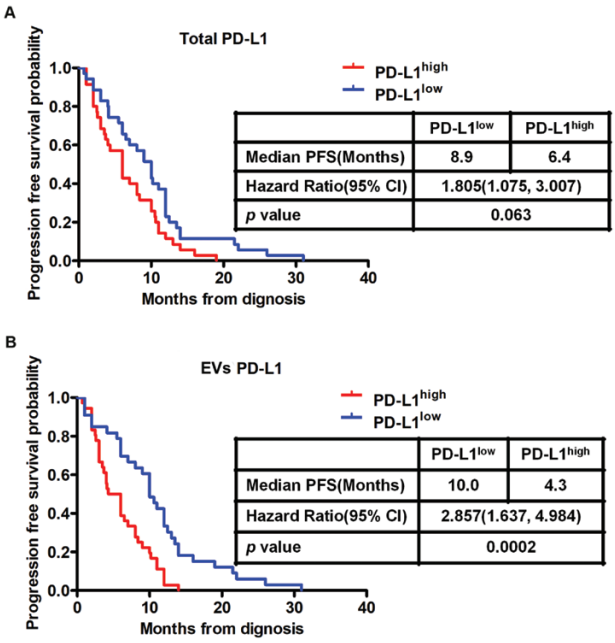

Figure 5: PD-L1$^+$ EVs can be used as a marker of progression-free survival in SCLC. Kaplan–Meier estimates of progression-free survival (PFS) in patients according to total PD-L1 (n = 70, P = 0.063) (A) or exosomal PD-L1 (n = 70, P = 0.0002) (B). HR, hazard ratio; CI, confidence interval.

to quantitatively investigate EVs PD-L1 in clinical samples, highlighting the need to develop EVs extraction methods amenable to use in clinical contexts.

The assessment of PD-L1 expression in circulating EVs has been evaluated in melanoma and head and neck cancer for its potential capability to guide the selection of patients to be treated with immunotherapy [24, 44]. It is worth noting that PD-L1 was also detected in microvesicles even though at a lower level [24]. Whether PD-L1 in microvesicles possesses diagnostic value or has communication with exosomal PD-L1 is all need to be validated with further experiments. Whether PD-L1 in EV-depleted plasma has communication with EVs PD-L1 needs further experiments to confirm.

Because PD-L1 expression varies among different types of lung cancers, we analyzed expression levels in a panel of human SCLC cell lines [50]. Our data revealed that only two of the six cell lines expressed PD-L1, which is consistent with clinical studies showing that PD-L1 is expressed at low levels in SCLC tumor tissues [13, 51]. Moreover, this may also explain the general lack of therapeutic response to anti-PD-L1 blockade in SCLC, which has led to less than optimistic expectations for the efficacy of ICI in this cancer.

We hypothesized that EVs PD-L1 may play a role in attenuating anti-tumor immunity in SCLC, as has been demonstrated in other cancers [25, 43, 52–54]. Indeed, we found that EVs from SCLC cells expressing high levels of PD-L1 induced downregulation of the T-cell activation marker CD69 on CD8$^+$ T cells, and also modulated the release of various cytokines from stimulated cells. These results support the possibility that EV PD-L1 could alter the immune microenvironment in SCLC, similar to findings in other cancers [19, 55]. More importantly, suppression of immunity may explain the association between EV PD-L1 and many clinicopathological characteristics of SCLC patients. However, we should note that we evaluated PBMCs, which contain various immune cells. In a future study, we will focus on exploring how EV PD-L1 may affect T cells and natural killer cells specifically.

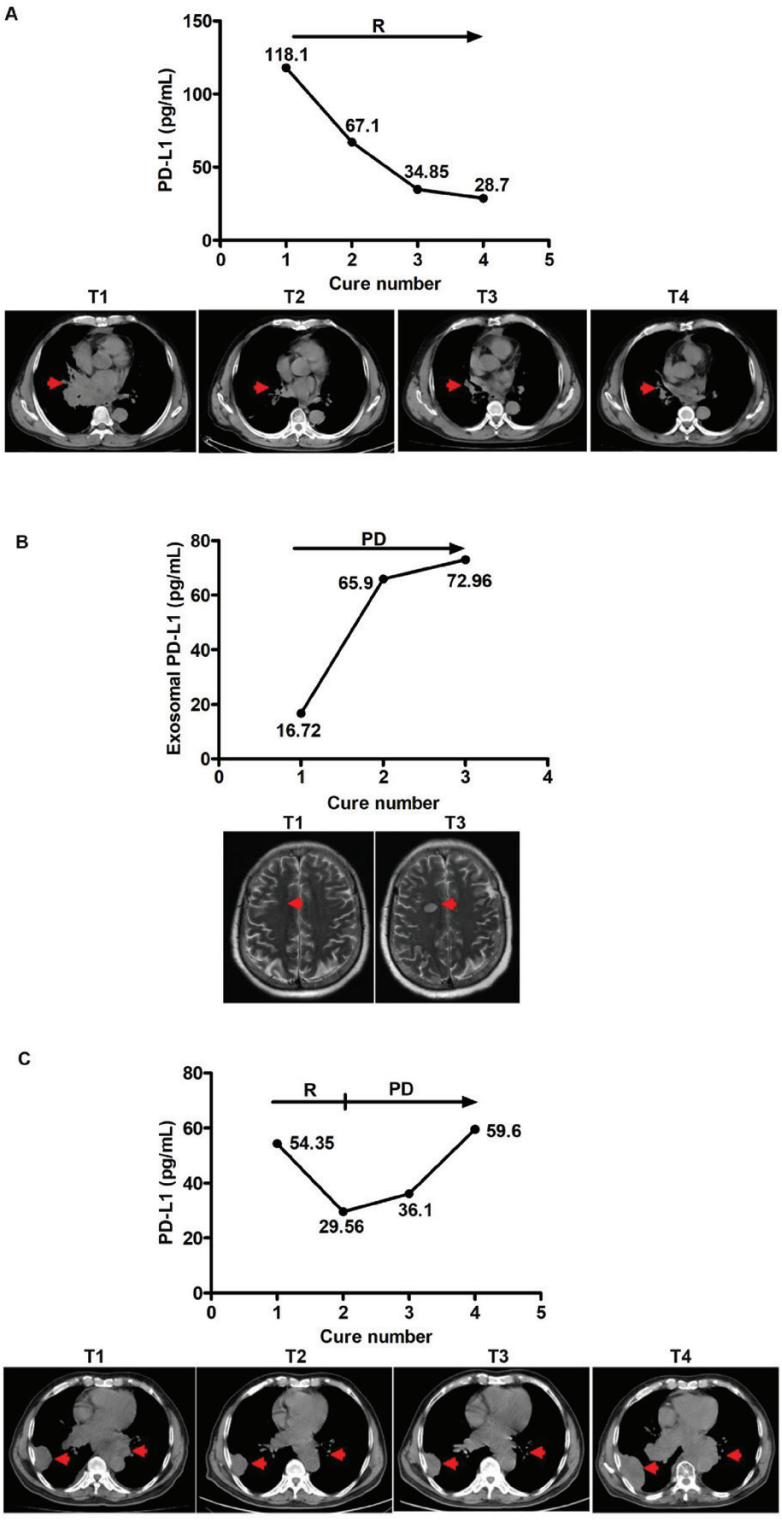

Figure 6: Circulating PD-L1⁺ EVs can be used as follow-up markers in SCLC patients. Case study of the correlation between EV PD-L1 levels in plasma samples from SCLC patients and response to therapy. Concomitant imaging and EV PD-L1 sampling in three patients experiencing (A) response as observed in the hilar on CT scan; (B) tumor metastases to the brain by MRI scan; (C) initial response (at cure 1) then disease progression as detected in the hilar and pleura on CT scan. R: response, PD: progression of the disease. Tumor sites in the scans are indicated by a red arrow.

Conclusion

To be summarized, our findings demonstrated that PD-L1 selectively expressed on SCLC tumor cells. In our work, as shown in Fig. 7, EVs can be naturally released from SCLC cells and enriched in immunosuppressive proteins, such as PD-L1. Additionally, EVs containing PD-L1 efficiently blocked CD3/CD28-stimulated T-cell activation and cytokines secretion. Importantly, a specific antibody of PD-L1 can significantly reverse the EV-mediated inhibition of CD8⁺ T-cell activation. At last, our study presents the evidence that circulating EVs

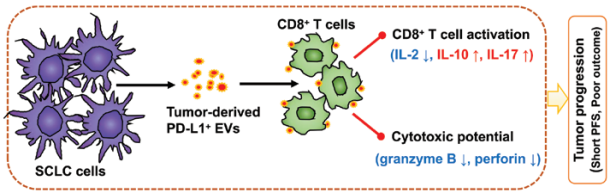

Figure 7: Graphical abstract of PD-L1⁺ EVs in immune regulation. SCLC cell lines release EVs expressing membrane PD-L1. PD-L1⁺ EVs released by SCLC cells inhibit CD8⁺ T cells activation and cytotoxicity. SCLC patients containing higher PD-L1⁺ EVs significantly correlated with short progression-free survival. Molecules shown in green stimulate immune activation; molecules shown in red are immunosuppressive marker.

containing PD-L1 could serve as a marker for cancer diagnosis, for monitoring therapeutic responses, and for predicting the prognosis in SCLC patients. Our study not only identifies SCLC tumor cell-derived EVs containing PD-L1 play an important role in the communication between extracellular environment and immune system, but also provides foundational evidence establishing the promising potential for the use of EV PD-L1 in the development of a novel anticancer approach.

Acknowledgments

We would like to thank Yinmei Li and Lei Gong (The University of Science and Technology of China, Hefei, Anhui, China) for the single extracellular vesicles capture. We thank Min Cheng (The First Affiliated Hospital of University of Science and Technology of China, Hefei, Anhui, China) for helpful advice on the FACS tests. We thank Anne M. O'Rourke, PhD, from Liwen Bianji, Edanz Group China (www.liwenbianji.cn/ac), for editing the English text of a draft of this manuscript. We thank the researchers in NanoFCM Inc. of Xiamen with experimental assistance.

Funding

This study was supported by the Fundamental Research Funds for the Central University (grant number WK9110000025, WK9110000075, WK9110000085), the National Cancer Center Climbing Funds (grant number NCC201812B036), the Natural Science Foundation of Anhui Province (grant number 2008085MH288), the National Ministry of Industry and Information Technology Science and Technology (grant number 2018MND102041).

Conflict of interest

The authors declare no conflicts of interest.

Authors' contributions

ML designed the study and reviewed the manuscript. XD and YH carried out most of the experiments and drafted the manuscript. FC performed the statistical analysis and assisted with experimental performance. ZC collected patients' clinical data. All authors read and approved the final manuscript.

Ethics approval and consent to participate

The study design was approved by the Institutional Review Board of Western Branch of The First Affiliated Hospital of University of Science and Technology of China, and written informed consent was obtained from all subjects enrolled in the study. Consent for publication: Not applicable.

Data availability

The datasets used or analyzed during the current study are available from the corresponding author upon reasonable request. Code availability: not applicable.

References

1. Siegel RL, Miller KD, Jemal A. Cancer statistics, 2019. *CA Cancer J Clin* 2019, 69, 7–34.
2. Altan M, Chiang AC. Management of small cell lung cancer: progress and updates. *Cancer J* 2015, 21, 425–33.
3. Network NCC. Clinical practice guidelines in oncology. Small cell lung cancer. Version 1.2018. https://www.nccn.org/professionals/physician_gls/default.aspx. 2017.
4. Reck M, Bondarenko I, Luft A, Serwatowski P, Barlesi F, Chacko R, et al. Ipilimumab in combination with paclitaxel and carboplatin as first-line therapy in extensive-disease-small-cell lung cancer: results from a randomized, double-blind, multicenter phase 2 trial. *Ann Oncol* 2013, 24, 75–83.
5. Hamilton G, Rath B. Immunotherapy for small cell lung cancer: mechanisms of resistance. *Expert Opin Biol Ther* 2019, 19, 423–32.
6. Sharma P, Hu-Lieskovan S, Wargo JA, Ribas A. Primary, adaptive, and acquired resistance to cancer immunotherapy. *Cell* 2017, 168, 707–23.
7. Ribas A, Hamid O, Daud A, Hodi FS, Wolchok JD, Kefford R, et al. Association of pembrolizumab with tumor response and survival among patients with advanced melanoma. *JAMA* 2016, 315, 1600–9.
8. Hodi FS, Chiarion-Sileni V, Gonzalez R, Grob JJ, Rutkowski P, Cowey CL, et al. Nivolumab plus ipilimumab or nivolumab alone versus ipilimumab alone in advanced melanoma (CheckMate 067): 4-year outcomes of a multicentre, randomised, phase 3 trial. *Lancet Oncol* 2018, 19, 1480–92.
9. Robert C, Thomas L, Bondarenko I, O'Day S, Weber J, Garbe C, et al. Ipilimumab plus dacarbazine for previously untreated metastatic melanoma. *N Engl J Med* 2011, 364, 2517–26.
10. Zhou K, Zhou J, Huang J, Zhang N, Bai L, Yang Y, et al. Cost-effectiveness analysis of atezolizumab plus chemotherapy in the first-line treatment of extensive-stage small-cell lung cancer. *Lung Cancer* 2019, 130, 1–4.
11. Horn L, Mansfield AS, Szczęsna A, Havel L, Krzakowski M, Hochmair MJ, et al; IMpower133 Study Group. First-line atezolizumab plus chemotherapy in extensive-stage small-cell lung cancer. *N Engl J Med* 2018, 379, 2220–9.
12. Iams WT, Porter J, Horn L. Immunotherapeutic approaches for small-cell lung cancer. *Nat Rev Clin Oncol* 2020, 17, 300–12.
13. Gadgeel SM, Pennell NA, Fidler MJ, Halmos B, Bonomi P, Stevenson J, et al. Phase II study of maintenance pembrolizumab in patients with extensive-stage small cell lung cancer (SCLC). *J Thorac Oncol* 2018, 13, 1393–9.
14. Kaunitz GJ, Cottrell TR, Lilo M, Muthappan V, Esandrio J, Berry S, et al. Melanoma subtypes demonstrate distinct PD-L1 expression profiles. *Lab Invest* 2017, 97, 1063–71.
15. Poggio M, Hu T, Pai CC, Chu B, Belair CD, Chang A, et al. Suppression of exosomal PD-L1 induces systemic anti-tumor immunity and memory. *Cell* 2019, 177, 414–427.e13.
16. Liu Y, Wang Y, Lv Q, Li X. Exosomes: from garbage bins to translational medicine. *Int J Pharm* 2020, 583, 119333.
17. Alyamani H, Obeid MA, Tate RJ, Ferro VA. Exosomes: fighting cancer with cancer. *Ther Deliv* 2019, 10, 37–61.
18. Zhang Y, Wang XF. A niche role for cancer exosomes in metastasis. *Nat Cell Biol* 2015, 17, 709–11.

19. Yang Y, Li CW, Chan LC, Wei Y, Hsu JM, Xia W, et al. Exosomal PD-L1 harbors active defense function to suppress T cell killing of breast cancer cells and promote tumor growth. *Cell Res* 2018, 28, 862–4.
20. Liu J, Fan L, Yu H, Zhang J, He Y, Feng D, et al. Endoplasmic reticulum stress causes liver cancer cells to release exosomal miR-23a-3p and up-regulate programmed death ligand 1 expression in macrophages. *Hepatology* 2019, 70, 241–58.
21. Sundararajan V, Sarkar FH, Ramasamy TS. The versatile role of exosomes in cancer progression: diagnostic and therapeutic implications. *Cell Oncol* 2018, 41, 223–52.
22. Surmiak M, Kosałka-Węgiel J, Polański S, Sanak M. Endothelial cells response to neutrophil-derived extracellular vesicles miRNAs in anti-PR3 positive vasculitis. *Clin Exp Immunol* 2021, 204, 267–82.
23. Xu R, Rai A, Chen M, Suwakulsiri W, Greening DW, Simpson RJ. Extracellular vesicles in cancer—implications for future improvements in cancer care. *Nat Rev Clin Oncol* 2018, 15, 617–38.
24. Chen G, Huang AC, Zhang W, Zhang G, Wu M, Xu W, et al. Exosomal PD-L1 contributes to immunosuppression and is associated with anti-PD-1 response. *Nature* 2018, 560, 382–6.
25. Gao L, Wang L, Dai T, Jin K, Zhang Z, Wang S, et al. Tumor-derived exosomes antagonize innate antiviral immunity. *Nat Immunol* 2018, 19, 233–45.
26. Cordonnier M, Nardin C, Chanteloup G, Derangere V, Algros MP, Arnould L, et al. Tracking the evolution of circulating exosomal-PD-L1 to monitor melanoma patients. *J Extracell Vesicles* 2020, 9, 1710899.
27. Tian Y, Gong M, Hu Y, Liu H, Zhang W, Zhang M, et al. Quality and efficiency assessment of six extracellular vesicle isolation methods by nano-flow cytometry. *J Extracell Vesicles* 2020, 9, 1697028.
28. Del Re M, Marconcini R, Pasquini G, Rofi E, Vivaldi C, Bloise F, et al. PD-L1 mRNA expression in plasma-derived exosomes is associated with response to anti-PD-1 antibodies in melanoma and NSCLC. *Br J Cancer* 2018, 118, 820–4.
29. Ludwig S, Floros T, Theodoraki MN, Hong CS, Jackson EK, Lang S, et al. Suppression of lymphocyte functions by plasma exosomes correlates with disease activity in patients with head and neck cancer. *Clin Cancer Res* 2017, 23, 4843–54.
30. Coffelt SB, Kersten K, Doornebal CW, Weiden J, Vrijland K, Hau CS, et al. IL-17-producing γδ T cells and neutrophils conspire to promote breast cancer metastasis. *Nature* 2015, 522, 345–8.
31. Kindlund B, Sjöling Å, Yakkala C, Adamsson J, Janzon A, Hansson LE, et al. CD4+ regulatory T cells in gastric cancer mucosa are proliferating and express high levels of IL-10 but little TGF-β. *Gastric Cancer* 2017, 20, 116–25.
32. Qiao J, Liu Z, Dong C, Luan Y, Zhang A, Moore C, et al. Targeting tumors with IL-10 prevents dendritic cell-mediated CD8+ T cell apoptosis. *Cancer Cell* 2019, 35, 901–915.e4.
33. Smyth MJ, Thia KY, Street SE, MacGregor D, Godfrey DI, Trapani JA. Perforin-mediated cytotoxicity is critical for surveillance of spontaneous lymphoma. *J Exp Med* 2000, 192, 755–60.
34. Barry M, Heibein JA, Pinkoski MJ, Lee SF, Moyer RW, Green DR, et al. Granzyme B short-circuits the need for caspase 8 activity during granule-mediated cytotoxic T-lymphocyte killing by directly cleaving Bid. *Mol Cell Biol* 2000, 20, 3781–94.
35. Thiery J, Keefe D, Boulant S, Boucrot E, Walch M, Martinvalet D, et al. Perforin pores in the endosomal membrane trigger the release of endocytosed granzyme B into the cytosol of target cells. *Nat Immunol* 2011, 12, 770–7.
36. Kalluri R, LeBleu VS. The biology, function, and biomedical applications of exosomes. *Science* 2020, 367, eaau6977.
37. Jeppesen DK, Fenix AM, Franklin JL, Higginbotham JN, Zhang Q, Zimmerman LJ, et al. Reassessment of exosome composition. *Cell* 2019, 177, 428–445.e18.
38. Mathieu M, Martin-Jaular L, Lavieu G, Théry C. Specificities of secretion and uptake of exosomes and other extracellular vesicles for cell-to-cell communication. *Nat Cell Biol* 2019, 21, 9–17.
39. Keller MD, Ching KL, Liang FX, Dhabaria A, Tam K, Ueberheide BM, et al. Decoy exosomes provide protection against bacterial toxins. *Nature* 2020, 579, 260–4.
40. Yu S, Sha H, Qin X, Chen Y, Li X, Shi M, et al. EGFR E746-A750 deletion in lung cancer represses antitumor immunity through the exosome-mediated inhibition of dendritic cells. *Oncogene* 2020, 39, 2643–57.
41. Lehmann BD, Paine MS, Brooks AM, McCubrey JA, Renegar RH, Wang R, et al. Senescence-associated exosome release from human prostate cancer cells. *Cancer Res* 2008, 68, 7864–71.
42. Sandfeld-Paulsen B, Jakobsen KR, Bæk R, Folkersen BH, Rasmussen TR, Meldgaard P, et al. Exosomal proteins as diagnostic biomarkers in lung cancer. *J Thorac Oncol* 2016, 11, 1701–10.
43. Daassi D, Mahoney KM, Freeman GJ. The importance of exosomal PDL1 in tumour immune evasion. *Nat Rev Immunol* 2020, 20, 209–15.
44. Theodoraki MN, Yerneni SS, Hoffmann TK, Gooding WE, Whiteside TL. Clinical significance of PD-L1(+) exosomes in plasma of head and neck cancer patients. *Clin Cancer Res* 2018, 24, 896–905.
45. Lux A, Kahlert C, Grützmann R, Pilarsky C. c-Met and PD-L1 on circulating exosomes as diagnostic and prognostic markers for pancreatic cancer. *Int J Mol Sci* 2019, 20, 3305.
46. Michaelidou K, Agelaki S, Mavridis K. Molecular markers related to immunosurveillance as predictive and monitoring tools in non-small cell lung cancer: recent accomplishments and future promises. *Expert Rev Mol Diagn* 2020, 20, 335–44.
47. Theodoraki MN, Matsumoto A, Beccard I, Hoffmann TK, Whiteside TL. CD44v3 protein-carrying tumor-derived exosomes in HNSCC patients' plasma as potential noninvasive biomarkers of disease activity. *Oncoimmunology* 2020, 9, 1747732.
48. Choo YW, Kang M, Kim HY, Han J, Kang S, Lee JR, et al. M1 macrophage-derived nanovesicles potentiate the anticancer efficacy of immune checkpoint inhibitors. *ACS Nano* 2018, 12, 8977–93.
49. Theodoraki MN, Yerneni S, Gooding WE, Ohr J, Clump DA, Bauman JE, et al. Circulating exosomes measure responses to therapy in head and neck cancer patients treated with cetuximab, ipilimumab, and IMRT. *Oncoimmunology* 2019, 8, 1593805.
50. Carvajal-Hausdorf D, Altan M, Velcheti V, Gettinger SN, Herbst RS, Rimm DL, et al. Expression and clinical significance of PD-L1, B7-H3, B7-H4 and TILs in human small cell lung Cancer (SCLC). *J Immunother Cancer* 2019, 7, 65.
51. Zhao X, Kallakury B, Chahine JJ, Hartmann D, Zhang Y, Chen Y, et al. Surgical resection of SCLC: prognostic factors and the tumor microenvironment. *J Thorac Oncol* 2019, 14, 914–23.
52. Fan Y, Che X, Qu J, Hou K, Wen T, Li Z, et al. Exosomal PD-L1 retains immunosuppressive activity and is associated with gastric cancer prognosis. *Ann Surg Oncol* 2019, 26, 3745–55.
53. Jiao S, Subudhi SK, Aparicio A, Ge Z, Guan B, Miura Y, et al. Differences in tumor microenvironment dictate T helper lineage polarization and response to immune checkpoint therapy. *Cell* 2019, 179, 1177–1190.e13.
54. Kim DH, Kim H, Choi YJ, Kim SY, Lee J-E, Sung KJ, et al. Exosomal PD-L1 promotes tumor growth through immune escape in non-small cell lung cancer. *Exp Mol Med* 2019, 51.
55. Ricklefs FL, Alayo Q, Krenzlin H, Mahmoud AB, Speranza MC, Nakashima H, et al. Immune evasion mediated by PD-L1 on glioblastoma-derived extracellular vesicles. *Sci Adv* 2018, 4, eaar2766.